J Optim Theory Appl
DOI 10.1007/s10957-013-0330-8

Optimal Kinematics of a Looped Filament

Francesca Maggioni · Florian A. Potra · Marida Bertocchi

Received: 6 October 2012 / Accepted: 2 May 2013

Abstract New kinematics of supercoiling of closed filaments as solutions of the elastic energy minimization are proposed. The analysis is based on the thin rod approximation of the linear elastic theory, under conservation of the self-linking number. The elastic energy is evaluated by means of bending contribution and torsional influence. Time evolution functions are described by means of piecewise polynomial transformations based on cubic spline functions. In contrast with traditional interpolation, the parameters, which define the cubic splines representing the evolution functions, are considered as the unknowns in a nonlinear optimization problem. We show how the coiling process is associated with conversion of mean twist energy into bending energy through the passage by an inflexional configuration in relation to geometric characteristics of the filament evolution. These results provide new insights on the folding mechanism and associated energy contents and may find useful applications in folding of macromolecules and DNA packing in cell biology.

Keywords Kinematics of curves · DNA supercoiling · Writhing · Twist · Deformation energy · Nonlinear optimization · Cubic B-spline representation

F. Maggioni (✉) · M. Bertocchi
Department of Mathematics, Statistics, Computer Science and Applications, University of Bergamo, Via dei Caniana 2, 24127 Bergamo, Italy
e-mail: francesca.maggioni@unibg.it

M. Bertocchi
e-mail: marida.bertocchi@unibg.it

F.A. Potra
Department of Mathematics & Statistics, University of Maryland, Baltimore, Baltimore County, MD 21250, USA
e-mail: potra@umbc.edu

Published online: 17 May 2013

1 Introduction

In this paper, we propose a novel mathematical method to investigate geometric and energetic aspects of the supercoiling process of closed filaments for DNA modeling.

Supercoiling phenomena play a key role in DNA. Many DNAs in bacteria, viruses and mitochondrion are found in the form of loops. The looped DNAs often wind in space to form intricate structures, in which case they are said to be supercoiled [1]. It is an interesting fact that a large fraction of DNAs exhibit some form of supercoiling in at least one stage of their life cycles. During biological processes such as transcription or replication, various mechanical forces act on the DNA and cause its underwinding or overwinding that results in the supercoiled configuration.

Geometric information plays a crucial role in relation to topology [2, 3]. DNA topology in vivo is extremely diverse. In bacteria, circular plasmids are condensed by supercoiling the DNA into highly writhed superhelical structures. Families of topoisomerase and gyrase enzymes alter the level of supercoiling by transiently introducing single or double strand breaks and changing the number of times the two strand of the duplex are wrapped around each other. Variation in DNA topology influences promoter activity, and is consequently involved in the regulation of gene expression and replication [4–7].

The kinematics of coil formation has been already analyzed in [8] and [9] by means of a set of governing equations, which prescribed the time-dependent evolutions of curves generated by epicycloids and hypocycloids and compared in terms of geometric and energetic aspects.

It was shown that high degree of coiling may be achieved at relatively low energy costs through appropriate folding and twist distribution, and independently from the number of coils formed. However, this class of curve evolutions represents just one parameter group embedded in an infinite-dimensional family of kinematically possible deformations; there may well exist other paths in the space of curve deformations, that may be energetically preferable favoring the formation of coils. This issue will be addressed in the present paper in the case of elastic filaments.

We propose to extend the model by determining time-dependent curves, which establish kinematic changes for which the filament's energy decreases monotonically, favoring folding.

The approach is based on the idea that the curve will adopt increasingly complex axial morphologies in order to lower its associated elastic energy. This change is mediated by the conversion of energy associated with the twisted nature of the elastic filament to the energy associated with its bending. For such thin filaments, it is necessary to ensure that this change respects the topology of the twisted rods (through conservation of the linking), under the assumption that the filament cannot pass through itself without the action from an outside influence (topoisomerase molecules in the biological context). We define an optimization problem, which simultaneously ensures that the elastic filament contorts to a lower energy whilst respecting the topology of the system and can be used to model the time dependent changing state of the system. Time evolution functions are described by means of piecewise polynomial transformations based on cubic B-spline functions. Moreover, in contrast with traditional interpolation, where values at grids points (vertices) have to match some

given values, we consider the parameters defining the evolution functions as part of the unknowns in a nonlinear optimization problem.

The model can be considered to explore geometric and topological aspects of the phenomenon of writhing or coiled instability observed in twisting elastic filaments. The energetics of the circular uniformly twisted equilibrium configuration was analyzed in the context of elastic rod theory by [10] and rediscovered by [11], (see [12]) and, more recently, in [13] and [14] in an elastic model for DNA, indicating that, for a certain critical total twist, this configuration no longer has minimum energy. For small values of the twist, the twisted ring is stable and conversely, for sufficiently high twist, the elastic ring becomes unstable and will start writhing out of the plane. The study of twisted elastic rings became of interest also in biophysics, when it was first realized that geometric and topological characterizations of curves could be of importance to understand DNA configurations [15]. While the static theory of supercoiled circular DNA has been studied extensively using elastic-rod models incorporating both elastic potential and electrostatic forces (e.g., [16–20], their dynamics has been studied using the dynamic Kirchhoff equations, as extensively detailed in [21] and [22]. With regard to computational methods, during the past years, a variety of diverse and complementary approaches have been presented [23], offering new physical and biological insights into fundamental functional processes of DNA. Analytical approaches have probed deeper into the effects of entropy and thermal fluctuations on DNA structure and on various topological constraints induced by DNA-binding proteins. New kinetic approaches—by molecular, Langevin, and Brownian dynamics, as well as extensions of elastic-rod theory—have begun to offer dynamic information associated with supercoiling [24, 25].

The paper is organized as follows: In the next section, we recall the kinematics models of multiple coiling analyzed in [8] and [9], where the time dependence was prescribed. Section 3 discusses geometric, topological, and energetic measures of filament coiling. Section 4 presents the model, and Sect. 5 the methodology adopted to solve it in terms of cubic B-spline functions. Numerical results in the case of single coil formation are presented in Sect. 6, in which geometric characteristics of the filament evolution in relation to the occurrence of an inflexional configuration are analyzed. Section 7 concludes the paper.

2 Kinematics of Supercoiling

The filament folding mechanism is investigated, improving a simple kinematic model for the dynamic evolution of an inextensible closed curve $\mathcal{C}$ in three-dimensional space introduced in [8] and [9]. For simplicity, the model covers a specific class of accessible morphologies connected isotopically to the initial twisted circular state: the curve evolution is generated by the simplest extension to three-dimensions of well-known planar curves *epicycloids* and *hypocycloids* (see [26, 27]) defined in the xy-projection. The curve is given by a smooth (at least C^3), simple (i.e., non-self-intersecting), closed curve with parametric equation $\mathbf{X} = \mathbf{X}(\xi, t)$ in $\mathbb{R}^3$, where $\xi \in [0, 2\pi]$ parametrizes the points along the curve and where t is a kinematic parameter (typically the time).

The time-dependent curve $\mathbf{X} = \mathbf{X}(\xi, t)$ is then described by the following model, which belongs to the family of *Fourier knots* (see [28]):

$$\mathbf{X} = \mathbf{X}(\xi, t): \quad \begin{cases} x = [a_1(t)\cos(n_1\xi) + a_2(t)\cos(n_2\xi)], \\ y = [a_3(t)\sin(n_1\xi) + a_4(t)\sin(n_2\xi)], \\ z = [a_5(t)\sin(\xi)], \end{cases} \tag{1}$$

where the integer parameters $n_2 > n_1 > 0$ control the number of coils produced and $a_i(t),\ i = 1, \ldots, 5$ are time-dependent functions.

In order to ensure inextensibility, each $\mathbf{X}$-component is normalized by the length function:

$$l(t) = \frac{1}{2\pi}\int_0^{2\pi}\left[\left(\frac{\partial x}{\partial \xi}\right)^2 + \left(\frac{\partial y}{\partial \xi}\right)^2 + \left(\frac{\partial z}{\partial \xi}\right)^2\right]^{1/2} \mathrm{d}\xi, \tag{2}$$

and (1) is then replaced by:

$$\mathbf{X} = \mathbf{X}(\xi, t): \quad \begin{cases} x = [a_1(t)\cos(n_1\xi) + a_2(t)\cos(n_2\xi)]/l(t), \\ y = [a_3(t)\sin(n_1\xi) + a_4(t)\sin(n_2\xi)]/l(t), \\ z = [a_5(t)\sin(\xi)]/l(t). \end{cases} \tag{3}$$

For simplicity, in [8] and [9], both constant and linear forms of the time-dependent functions $a_i(t),\ i = 1, \ldots, 5$ were considered with:

$$a_1(t) = a_3(t) = 1, \qquad a_2(t) = a_4(t) = a_5(t) = \pm t,$$

referring to epicycloid or hypocycloid type of curve in relation to the corresponding type of plane curve in the xy-projection. With the above prescription, the equations in (3) describe the time evolution of closed curves with initial condition ($t = 0$) chosen in order to originate from a plane circle of length $L = 2\pi$, and to evolve to form single coiled (see Fig. 1) or supercoiled configurations (see Fig. 2 in the case of 5 coils). The coil is produced by folding the curve in space through the development of a loop region that gives rise to the full coil. This type of deformation is known as *Reidemeister type I move* and it leaves the topology of the curve unchanged.

Conversely, an appropriate time-dependent prescription should be dictated by the specific physical process considered. The particular time-dependent class of curves chosen in [8] and [9] to represent the coil transition are, in fact, just one-parameter

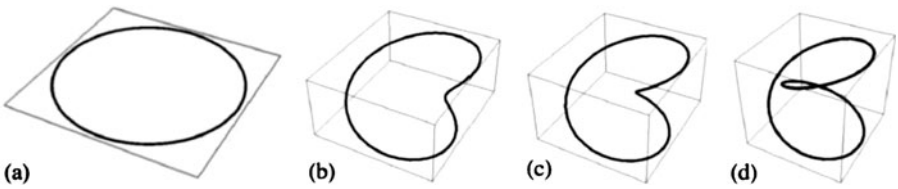

Fig. 1 Single coil formation generated by (3) for $n_1 = 1$ and $n_2 = 2$ and kinematic parameters $a_1(t) = a_3(t) = 1, a_2(t) = a_4(t) = -t$, and $a_5(t) = t$. The initial circular configuration (**a**) writhes and folds in space (**b**)–(**c**) to produce the final coil (**d**)

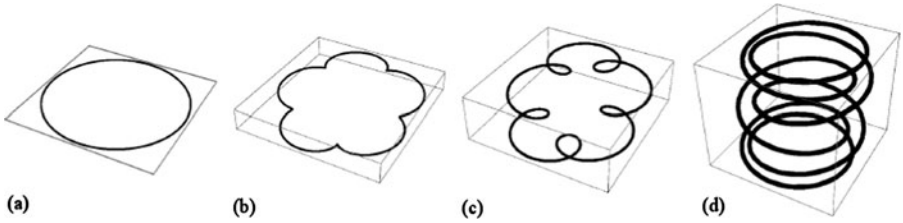

Fig. 2 Five coil formations generated by (3) for $n_1 = 1$ and $n_2 = 6$ and kinematic parameters $a_1(t) = a_3(t) = 1, a_2(t) = a_4(t) = -t$, and $a_5(t) = t$. The initial circular configuration (**a**) writhes and folds in space in 5 different places (**b**)–(**c**) to produce 5 final coils (**d**)

groups embedded in an infinite-dimensional family of kinematically possible deformations. There may well exist other paths in the space of curve deformations that may be energetically preferable: this will be addressed in the present paper in the context of elastic filaments. We will determine the time-dependent functions $a_i(t), i = 1, \ldots, 5$ such that the curve deformations (3) are energetically preferred in terms of minimizing the elastic energy functional.

3 Measures and Energetics of Supercoiling

The total amount of filament coiling, folding, and twisting is quantified by global geometric quantities such as the normalized total curvature, the writhing number, and twist. Let $c := c(\xi, t)$ denote the curvature and $\tau := \tau(\xi, t)$ the torsion of the curve $\mathbf{X}(t)$ through the standard *Frenet–Serret formulae* at time t:

$$\begin{pmatrix} \hat{\mathbf{t}}'(\xi,t) \\ \hat{\mathbf{n}}'(\xi,t) \\ \hat{\mathbf{b}}'(\xi,t) \end{pmatrix} = \begin{pmatrix} 0 & c(\xi,t) & 0 \\ -c(\xi,t) & 0 & \tau(\xi,t) \\ 0 & -\tau(\xi,t) & 0 \end{pmatrix} \begin{pmatrix} \hat{\mathbf{t}}(\xi,t) \\ \hat{\mathbf{n}}(\xi,t) \\ \hat{\mathbf{b}}(\xi,t) \end{pmatrix}, \tag{4}$$

where the prime denotes differentiation with respect to ξ,

$$\hat{\mathbf{t}}(\xi,t) := \mathbf{X}'(\xi,t) / \left\| \mathbf{X}'(\xi,t) \right\|, \tag{5}$$

is the unit tangent to $\mathcal{C}(t)$ at ξ at time t, $\hat{\mathbf{n}} := \hat{\mathbf{t}}'/c$ is the unit principal normal vector and $\hat{\mathbf{b}} := \hat{\mathbf{t}} \times \hat{\mathbf{n}}$ the unit bi-normal vector such that the triple $\{\hat{\mathbf{t}}, \hat{\mathbf{n}}, \hat{\mathbf{b}}\}$ represents the *Frenet frame* on $\mathbf{X}$.

Coiling is naturally measured by the *normalized total curvature* $K(t)$, given by

$$K(t) := \frac{1}{2\pi} \oint_{\mathcal{C}} c(\xi,t) \left\| \mathbf{X}'(\xi,t) \right\| \mathrm{d}\xi, \tag{6}$$

where the factor $\|\mathbf{X}'(\xi, t)\|$ measures the length of the tangent vector $\mathbf{X}'(\xi, t)$ of the curve $\mathbf{X}$ at ξ at time t.

An important descriptor of *supercoiling* is given by the *writhing number* $\mathrm{Wr}(t)$ [15], defined by

$$\mathrm{Wr}(t) := \frac{1}{4\pi}\oint_{\mathcal{C}}\oint_{\mathcal{C}} \frac{\hat{\mathbf{t}}(\xi,t)\times\hat{\mathbf{t}}(\xi^*,t)\cdot[\mathbf{X}(\xi,t)-\mathbf{X}(\xi^*,t)]}{|\mathbf{X}(\xi,t)-\mathbf{X}(\xi^*,t)|^3} \times \left\|\mathbf{X}'(\xi,t)\right\|\left\|\mathbf{X}'\left(\xi^*,t\right)\right\| \mathrm{d}\xi\,\mathrm{d}\xi^*, \tag{7}$$

where $\mathbf{X}(\xi,t)$ and $\mathbf{X}(\xi^*,t)$ denote two points on the axis for any pair $\{\xi,\xi^*\}\in[0,2\pi]$ and the integration is performed twice on the same curve $\mathcal{C}(t)$.

A simple geometric interpretation of Wr is in terms of the algebraic sum of positive and negative crossings of the plane projection of the curve $\mathcal{C}(t)$.

Suppose we view the curve $\mathcal{C}(t)$ along the viewing direction $\boldsymbol{\nu}$. Let $n_+(\boldsymbol{\nu},t)$ be the number of positive crossings and $n_-(\boldsymbol{\nu},t)$ the number of negative crossings of the projected curve at time t, where we have assigned a positive or negative sign to each intersection site of the oriented diagram according to the orientation of the curve $\mathcal{C}(t)$.

Then

$$\mathrm{Wr}(t) = \left\langle n_+(\boldsymbol{\nu},t) - n_-(\boldsymbol{\nu},t)\right\rangle, \tag{8}$$

where the angular brackets denote averaging over all directions $\boldsymbol{\nu}$ of projection [15]. The writhing number depends only on the *geometry* of the curve $\mathcal{C}(t)$, it is invariant under rigid motions or dilations of the space containing the curve, its sign changes by reflection in a plane, it changes continuously under continuous deformations of $\mathcal{C}(t)$ over time and jumps by ±2 as the curve passes through itself.

A measure of the *winding* of the infinitesimal fibres around $\mathcal{C}(t)$ is given by the *total twist number* $\mathrm{Tw}(t)$ defined by

$$\mathrm{Tw}(t) := \frac{1}{2\pi}\oint_{\mathcal{C}} \Omega(\xi,t)\left\|\mathbf{X}'(\xi,t)\right\| \mathrm{d}\xi \tag{9}$$

$$= \frac{1}{2\pi}\int_{\mathcal{C}} \left(\hat{\mathbf{N}}(\xi,t)\times\hat{\mathbf{N}}'(\xi,t)\right)\cdot\hat{\mathbf{t}}(\xi,t)\left\|\mathbf{X}'(\xi,t)\right\| \mathrm{d}\xi, \tag{10}$$

where $\Omega = (\hat{\mathbf{N}}\times\hat{\mathbf{N}}')\cdot\hat{\mathbf{t}}$ is the *angular twist rate* and $\hat{\mathbf{N}}' = \frac{\mathrm{d}\hat{\mathbf{N}}}{\mathrm{d}\xi}$ (see [29]).

Tw can be decomposed as the sum of the normalized total torsion $\mathcal{T}(t)$ and the intrinsic twist $\mathcal{N}(t)$ of the fibers *around* $\mathcal{C}(t)$,

$$\mathrm{Tw}(t) := \frac{1}{2\pi}\oint_{\mathcal{C}} \tau(\xi,t)\left\|\mathbf{X}'(\xi,t)\right\| \mathrm{d}\xi + \frac{1}{2\pi}\left[\Theta(t)\right]_{\mathcal{F}} = \mathcal{T}(t)+\mathcal{N}(t), \tag{11}$$

where $\Theta(t)$ represents a rotation of the filament material body independent of the axial geometry. For simplicity, we take the fibers to be closed curves uniformly wound about $\mathcal{C}$. In this case $\mathcal{N}$ is an integer.

Tw is invariant under rigid motions or dilations of the space containing the filament, it is *additive* and it changes continuously, without any jump, under deformation of the filament in time, even if the axis curve passes through itself.

Note that K, Wr, and $\mathcal{T}$ depend only on the geometry of the filament axis, whereas the total twist Tw and the intrinsic twist $\mathcal{N}$ depend also on the distribution of the filament fibers.

According to the well-known Calugareanu–White formula [30, 31], the sum of $\mathrm{Wr}(t)$ and $\mathrm{Tw}(t)$ provides a topological invariant called the *linking number* Lk,

$$\mathrm{Lk} := \mathrm{Wr}(t) + \mathrm{Tw}(t), \tag{12}$$

which establishes a conservation of topology during the folding process through a continuous change of the filament geometry and conversion of twist Tw in Wr. This will be crucial for the energy of the system, characterized by a transfer of torsional energy to bending energy [32].

We analyze the energetics of folding by adopting the linear elastic theory for a uniformly homogeneous and isotropic filament of circular cross-section and inextensible length.

The elastic characteristics are specified by the bending stiffness K_b and the torsional stiffness K_t of the filament (which can be estimated from experimental measurements). The ratio $\chi = K_b/K_t$ lies between 1 (compressible material) and 1.5 (incompressible), with metals around 5/4. DNA filaments may present higher values of twist to bending rigidity.

The associated deformation energy can then be described in terms of bending and twisting components:

$$E(t) := E_b(t) + E_t(t) = \frac{1}{2}\oint_{\mathcal{C}} \left[K_b\big(c(\xi,t)\big)^2 + K_t\big(\Omega(\xi,t)\big)^2\right] \left\|\mathbf{X}'(\xi,t)\right\| \mathrm{d}\xi. \tag{13}$$

The bending energy $E_b(t)$ is due to curvature effects, and the torsional energy $E_t(t)$ is due to torsion and intrinsic twist.

Typically, it is supposed that the twist rate Ω is constant along the filament ($\Omega = \Omega_c$, relaxed state) and then the term $E_t(t)$ can be replaced by the *mean twist* energy $E_{\mathrm{tw}}(t)$ which, for a curve of length $L = 2\pi$, is given by

$$E_{\mathrm{tw}}(t) := E_t|_{\Omega_c}(t) = \frac{K_t L}{2}(\Omega_c)^2 = \pi K_t\big(\mathrm{Lk} - \mathrm{Wr}(t)\big)^2. \tag{14}$$

This simplification allows to base all the computation only on the geometry of the curve $\mathbf{X}$.

Normalizing each term with respect to a reference configuration energy E_0, associated to the circular configuration of radius $R_0 = c_0^{-1} = 1$ and zero twist $E_0 = \pi K_b$, the relative total energy takes the form:

$$\tilde{E}(t) := \tilde{E}_b(t) + \tilde{E}_{tw}(t) = \frac{1}{2\pi}\oint_{\mathcal{C}} \big(c(\xi,t)\big)^2 \left\|\mathbf{X}'(\xi,t)\right\| \mathrm{d}\xi + \frac{(\mathrm{Lk} - \mathrm{Wr}(t))^2}{\chi}. \tag{15}$$

4 Coiling Formation Under Elastic Energy Minimization

In case the coiling process is favored, the total energy $\tilde{E}(t)$ (15) is monotonically decreasing in time, attaining at $t = 0$ its smallest value $\tilde{E}_0$. From (15) we get

$$\tilde{E}_0 := \tilde{E}(0) = 1 + \frac{\mathrm{Lk}^2}{\chi}, \tag{16}$$

which depends quadratically on Lk.

In [9], for prescribed time evolution, such a monotonically decreasing behavior was obtained by changing the linking number Lk (or twist Tw since at $t = 0$ $\mathrm{Wr} = 0$) of the filament structure. For the single coil case, it was found that, with $\mathrm{Lk} \geq 9$, the total energy always decreases, independently of χ, hence favoring coiling. However, it should be admitted here that the imposed condition on initial linking to provide spontaneous coiling is sufficient, but not necessary.

In addition, the critical twist value Tw_c to generate the *writhing instability* where the (unstable) twisted ring folds out of the plane has been identified by [10] and rediscovered by [11]:

$$\mathrm{Tw}_c = \frac{\sqrt{3}}{R}\chi. \tag{17}$$

This means that a circular filament of unitary radius R becomes unstable when it has been twisted by about two full turns (with limits 1.73 to 2.6 corresponding to χ between 1 and 1.5).

This important information will be taken into account in the following model which determines the time-dependent functions $a_i(t), i = 1, \ldots, 5$ in (3) such that the coiling process is energetically preferred in terms of elastic deformation energy. In order to emphasize the dependence on the time-dependent functions $a_i(t), i = 1, \ldots, 5$, we consider the time-dependent vector function

$$a(t) = \big(a_1(t), a_2(t), a_3(t), a_4(t), a_5(t)\big) \tag{18}$$

and write $\tilde{E}(a(t)), l(a(t)), \ldots$ instead of $\tilde{E}(t), l(t), \ldots$.

The problem is modeled as follows:

$$\min_{a_1(t),\ldots,a_5(t)} \int_{t_0}^{t_{\mathrm{fin}}} \tilde{E}\big(a(t)\big)\,\mathrm{d}t \tag{19}$$

$$\text{s.t.} \quad \frac{\mathrm{d}}{\mathrm{d}t}\tilde{E}\big(a(t)\big) \leq 0, \quad \forall t \in [t_0, t_{\mathrm{fin}}], \tag{20}$$

$$\tilde{E}\big(a(t_0)\big) = \tilde{E}_0, \tag{21}$$

$$l\big(a(t)\big) = 2\pi, \quad \forall t \in [t_0, t_{\mathrm{fin}}]; \tag{22}$$

it represents the minimization along the time interval $[t_0, t_{\mathrm{fin}}]$ of normalized total energy $\tilde{E}(a(t)) = \tilde{E}_b(a(t)) + \tilde{E}_{tw}(a(t))$ with respect to the time-dependent functions $a_i(t), i = 1, \ldots, 5$ (see (18)). Problem (19)–(22) finds the state variables $a_i(t)$ such that the total elastic energy $\tilde{E}$ is minimized in $[t_0, t_{\mathrm{fin}}]$. $\tilde{E}$ is monotonically decreasing in time (20) favoring coiling, it satisfies the initial condition (21) corresponding to a circle of unitary radius and, and the length $l(t)$ of the filament is kept constant (22).

5 Numerical Methods

Problem (19)–(22) is solved by considering the corresponding discrete version obtained partitioning the time interval $[t_0, t_{\mathrm{fin}}] = [t_0, t_F]$ into F sub-intervals of width

$q = \frac{t_{\text{fin}} - t_0}{F}$ through points t_f:

$$\min_{a_1(t),\ldots,a_5(t)} q\left[\frac{\tilde{E}(t_0)+\tilde{E}(t_F)}{2}+\sum_{f=1}^{F-1}\tilde{E}\big(a(t_f)\big)\right]+\gamma\sum_{f=0}^{F}p(t_f)+\mu\sum_{f=1}^{F-1}h(t_f) \quad (23)$$

$$\text{s.t.} \quad \tilde{E}\big(a(t_f)\big) \geq \tilde{E}\big(a(t_{f+1})\big), \quad f = 0,\ldots,F-1, \quad (24)$$

$$\tilde{E}\big(a(t_0)\big) = \tilde{E}_0, \quad (25)$$

$$l\big(a(t_f)\big) = 2\pi, \quad f = 0,\ldots,F, \quad (26)$$

where the objective function (23) includes the integral in (19) computed according to the trapezoidal rule [33] and two penalizations terms imposed to smooth the state variables: one on the *norm* of the vector $a(t_f)$ with cost γ given by

$$p(t_f) = \sum_{i=1}^{5} a_i^2(t_f), \quad f = 0,\ldots,F, \quad (27)$$

and one on the *curvature* of $a_i(t_f)$, $i = 1,\ldots,5$ with cost $\mu < \gamma$, by means of the central difference approximation of the second derivative

$$k\big(a_i(t_f)\big) = \frac{\frac{a_i(t_{f+1})-a_i(t_f)}{t_{f+1}-t_f} - \frac{a_i(t_f)-a_i(t_{f-1})}{t_f-t_{f-1}}}{t_{f+1}-t_{f-1}}, \quad f = 1,\ldots,F-1, \quad (28)$$

and

$$h(t_f) = \sum_{i=1}^{5} k\big(a_i(t_f)\big)^2, \quad f = 1,\ldots,F-1. \quad (29)$$

The unknowns in the optimization problem (23)–(26) are the parameters defining the functions $a_1(t),\ldots,a_5(t)$. In this paper, we will represent these functions in terms of B-splines, and therefore the unknowns of our optimization problem will be the corresponding de Boor points.

Note that the integrals along the curve $\mathcal{C}$ of the bending energy $\tilde{E}_b(a(t_f))$ and of the length function $l(a(t_f))$ in problem (23)–(26) have been computed by means of the trapezoidal rule [33] discretizing the axis into K segments: let b be the generic integrand function, then

$$\oint_{\mathcal{C}} b\,\mathrm{d}\xi \approx \frac{2\pi}{K}\left[\frac{b(0)+b(2\pi)}{2}+\sum_{k=1}^{K-1} b(\xi_k)\right]. \quad (30)$$

Moreover, the double integral along the curve $\mathcal{C}$ of the writhing number Wr (7), which contributes to the mean twist energy $\tilde{E}_{tw}(a(t_f))$, has been computed by means of the *double* trapezoidal rule: the domain rectangle

$$\mathcal{R} = \mathcal{C}\times\mathcal{C} = \big\{(\xi,\xi^*) : 0 \leq \xi \leq 2\pi, 0 \leq \xi^* \leq 2\pi\big\} \quad (31)$$

is divided into smaller sub-rectangles $\{\mathcal{R}_{k,r}\}$, $k = 1, \ldots, K$ and $r = 1, \ldots, R$ obtained as the intersections of the kth subinterval in $[0, 2\pi]$ with the rth subinterval in $[0, 2\pi]$. Denoting by b the integrand function in (7) yields

$$\begin{aligned}
&\oint_{\mathcal{C}} \oint_{\mathcal{C}} b \, \mathrm{d}\xi \, \mathrm{d}\xi^* \\
&\quad \approx \frac{4\pi^2}{KR} \left(2 \sum_{r=1}^{R-1} b(0, \xi_r) + 2 \sum_{r=1}^{R-1} b(2\pi, \xi_r) + 4 \sum_{r=1}^{R-1} \sum_{k=1}^{K-1} b(\xi_k, \xi_r) \right) \\
&\qquad + \frac{4\pi^2}{KR} \left(b(0,0) + b(0, 2\pi) + b(2\pi, 0) + b(2\pi, 2\pi) + 2 \sum_{k=1}^{K-1} b(\xi_k, 0) \right. \\
&\qquad \left. + 2 \sum_{k=1}^{K-1} b(\xi_k, 2\pi) \right),
\end{aligned}$$

also called the *four-corners method*.

Problem (23)–(26) is then solved in the case of single coil formation ($n_1 = 1$, $n_2 = 2$ in (3)) with length function $l(a(t)) = \int_{\mathcal{C}} \sqrt{\Psi(\xi, t)} \, \mathrm{d}\xi$, where

$$\begin{aligned}
\Psi(\xi, t) &= \sin^2(\xi) \big(a_1(t) + 4a_2(t) \cos(\xi) \big)^2 \\
&\quad + \big(a_3(t) \cos(\xi) + 2a_4(t) \cos(2\xi) \big)^2 + a_5^2(t) \cos^2(\xi),
\end{aligned}$$

and bending energy $\tilde{E}_b = \tilde{E}_b(a(t))$ given by

$$\begin{aligned}
\tilde{E}_b = \int_{\mathcal{C}} \big[& 12 \cos(\xi) \big(a_1^2 a_3 a_4 + a_1 a_2 \big(a_3^2 + 8a_4^2 + a_5^2 \big) + 8a_2^2 a_3 a_4 \big) \\
& + 3 \cos(2\xi) \big(a_4^2 \big(a_1^2 - a_5^2 \big) + 6a_1 a_2 a_3 a_4 + 5a_2^2 \big(a_3^2 + a_5^2 \big) \big) \\
& + 2a_1^2 a_3^2 - 4a_1^2 a_3 a_4 \cos(3\xi) - 6a_1^2 a_4^2 \cos(4\xi) + a_2^2 a_4^2 \cos(6\xi) \\
& + 10a_1^2 a_4^2 + 2a_1^2 a_5^2 + 4a_1 a_2 a_3^2 \cos(3\xi) - 2a_1 a_2 a_3 a_4 \cos(6\xi) \\
& + 48a_1 a_2 a_3 a_4 - 32a_1 a_2 a_4^2 \cos(3\xi) + 4a_1 a_2 a_5^2 \cos(3\xi) + 6a_2^2 a_3^2 \cos(4\xi) \\
& + a_2^2 a_3^2 \cos(6\xi) + 10a_2^2 a_3^2 + 32a_2^2 a_3 a_4 \cos(3\xi) + 128a_2^2 a_4^2 + 6a_2^2 a_5^2 \cos(4\xi) \\
& + a_2^2 a_5^2 \cos(6\xi) + 10a_2^2 a_5^2 - 6a_4^2 a_5^2 \cos(4\xi) - a_4^2 a_5^2 \cos(6\xi) + 10a_4^2 a_5^2 \big] \\
& / \big[2 \big(\sin^2(\xi) \big(a_1 + 4a_2 \cos(\xi) \big)^2 + \big(a_3 \cos(\xi) + 2a_4 \cos(2\xi) \big)^2 \\
& + a_5^2 \cos^2(\xi) \big)^{5/2} \big] \mathrm{d}\xi
\end{aligned}$$

approximated according to (30). According to the critical twist value (17), we set $\mathrm{Lk} = 3$ such that the mean twist energy $\tilde{E}_{tw}$ becomes:

$$\tilde{E}_{tw}\big(a(t)\big) = \big(3 - \mathrm{Wr}\big(a(t)\big)\big)^2 \tag{32}$$

with $\chi = 1$. Note that, to avoid the singularity in the integrand function of Wr for $\xi \to \xi^* + 2k\pi$ $(k = 0, 1)$, we set its value at the four vertices of the domain integration $\mathcal{R}$ equal to zero.

The initial $(t = 0)$ configuration in (3) is chosen to be a circle of unitary radius:

$$\mathbf{X} = \mathbf{X}(\xi, 0): \quad \begin{cases} x = \cos(\xi), \\ y = \sin(\xi), \\ z = 0, \end{cases} \tag{33}$$

obtained by setting

$$\big(a_1(0), a_2(0), a_3(0), a_4(0), a_5(0)\big) = (1, 0, 1, 0, 0), \tag{34}$$

with associated initial deformation energy $\tilde{E}_0 = 10$.

Time evolution functions $a_i(t)$, $i = 1, \ldots, 5$ in problem (23)–(26) are described by means of piecewise polynomial transformations based on cubic B-splines [34]. We briefly recall their definitions and main properties.

Let T be a nondecreasing sequence of knots $t_w \in [t_0, t_{\mathrm{fin}}] = [0, 1]$ known as the *knot vector*:

$$T = \{t_0, t_1, \ldots, t_m\}. \tag{35}$$

A B-spline of degree n is a parametric curve composed of a linear combination of basis B-splines $b_w^n(t)$ of degree n with $w = 0, \ldots, m - n - 1$. Kinematic functions $a_i(t)$ can be then described as follows

$$a_i(t) = \sum_{w=0}^{m-n-1} P_{i,w} b_w^n(t), \quad i = 1, \ldots, 5, \tag{36}$$

where $P_{i,w}$, $w = 0, \ldots, m - n - 1$, $i = 1, \ldots, 5$ are called *control points* or *de Boor points* forming a convex hull; the basis B-splines $b_w^n(t)$ are defined using the *Cox–de Boor recursion formula*:

$$b_w^0(t) = \begin{cases} 1, & \text{if } t_w < t < t_{w+1} \text{ and } t_w < t_{w+1}, \\ 0, & \text{otherwise}, \end{cases}$$

$$b_w^j(t) = \frac{t - t_w}{t_{w+j} - t_w} b_w^{j-1}(t) + \frac{t_{w+j+1} - t}{t_{w+j+1} - t_{w+1}} b_{w+1}^{j-1}(t), \quad j = 1, \ldots, n.$$

In the implementation, we consider a special case of non-periodic B-splines where the first $n + 1$ knots are equal to 0, the last $n + 1$ knots are equal to 1, and the internal knots $t_{n+1}, \ldots, t_{m-n-1}$ correspond to the grid points $t_0, \ldots, t_{\mathrm{fin}}$. We choose $n = 3$, which leads to cubic B-splines.

6 Numerical Results

Our numerical experiments were performed in the Mathematica 8.0 environment (http://www.wolfram.com/mathematica/). Problem (23)–(26) was solved by means of the *NMinimize* function which implements several algorithms for finding constrained global minima and chooses automatically what it believes to be the best algorithm for the given constrained optimization problem. For our problem, *NMinimize* chose the *Nelder–Mead Method*, a direct search method which does not use derivative information. For a description of this method, see, for example, [35]. We have also solved problem (23)–(26) by using the software package *Knitro release 7* (http://www.ziena.com/knitro.htm) under Mathematica 8.0. We took the solution obtained with the Nelder–Mead method as starting point and solved the problem via the *Interior Point Method* algorithm. In our computational experiments, we set $\mu = 0.001$, $\gamma = 0.1$. The time interval $[t_0, t_{\text{fin}}] = [0, 1]$ is divided into 4 sub-intervals of constant width 0.25. The single and double integrals in space for the computation of the length function and deformation energy were computed by the trapezoidal method dividing the curve into $K = 10$ segments and the domain $\mathcal{R} = \mathcal{C} \times \mathcal{C}$ into $KR = 100$ sub-rectangles. Problem (23)–(26) is solved in terms of B-spline representation with 30 free variables given by the control points $P_{i,w}$, $w = 1, \ldots, 6$, $i = 1, \ldots, 5$ in (36) and initial ($w = 0$) conditions

$$(P_{1,0}, P_{2,0}, P_{3,0}, P_{4,0}, P_{5,0}) = (1, 0, 1, 0, 0). \tag{37}$$

Note that the constraints (24)–(26) are enforced every 0.1 time units ($q = 0.1$ and $F = 10$). Consequently, the constraints of the problem consist of 12 nonlinear equalities and 10 nonlinear inequalities. The number of nonzero entries in the Jacobian is 365 and in the Hessian 465. The interior point method from Knitro needs 30 iterations to solve this problem, 285 conjugate gradient iterations, 112 function evaluations, 31 gradient evaluations, and 30 Hessian evaluations. The final absolute feasibility error is 1.01e−009 and final absolute optimality error 3.31e−007.

The execution time was 3181.66 seconds for the Nelder–Mead method and only 10.34 for Knitro using a personal computer VAIO Intel® Core™ i5 processor, Windows 7 Professional (64-bit) S Series, 4 GB Memory.

The optimal objective function value is 9.5, the optimal control points variables are reported in Table 1 and the optimal B-spline kinematic solutions are plotted in Figs. 3–11.

Figure 4 shows the total elastic energy $\tilde{E}(t)$ versus time t associated to the kinematics solution depicted in Fig. 11. Squared markers on the x-axis denote the grid points where the constraint (24) is enforced: the monotonic decreasing behavior is satisfied and, as expected, the largest value that is going to be relaxed is $\tilde{E}(0) = 10$. Contributions to the total deformation energy from bending and mean twist components are plotted in Fig. 5(a)–(b): $\tilde{E}_b(t)$ grows from $\tilde{E}_b(0) = 1$ associated to the initial circular configuration of unitary radius to 3 in the final state. Conversely, the mean twist energy $\tilde{E}_{tw}(t)$ decreases from $\tilde{E}_{tw}(0) = 9$ (since $\text{Wr}(0) = 0$) being related to the change in filament writhing.

The inextensibility constraint (26) is also satisfied as we can see from Fig. 6, which shows the filament length function $l(t)$ versus time $t \in [0, 1]$. As before, squared

Table 1 Optimal solutions of problem (23)–(26) solved in the case of single coil formation by means of the cubic B-spline function representation

$P_{i,w}$	$i=1$	$i=2$	$i=3$	$i=4$	$i=5$
$w=0$	1	0	1	0	0
$w=1$	0.908	0.061	0.98	−0.012	0.594
$w=2$	0.908	−0.241	0.984	−0.242	0.252
$w=3$	0.659	−0.258	0.811	−0.291	0.748
$w=4$	0.290	−0.151	0.611	−0.396	1.038
$w=5$	0.396	−0.462	0.373	−0.320	0.839
$w=6$	0.101	−0.166	0.331	−0.400	1.121

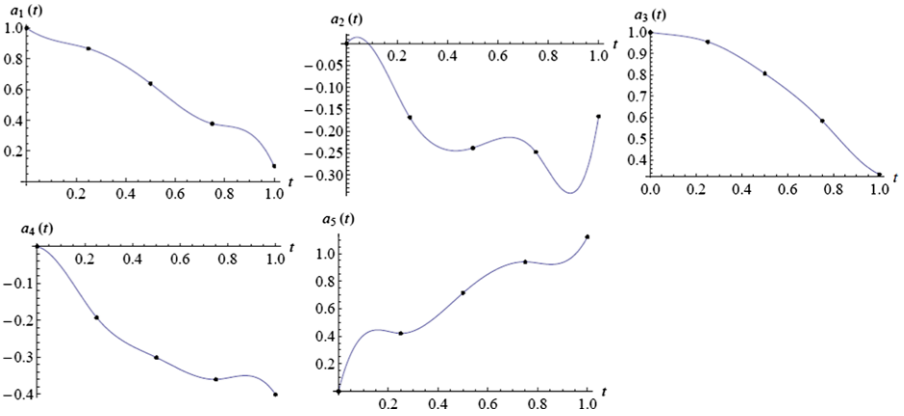

Fig. 3 Kinematic B-spline solutions $a_i(t)$ plotted versus time $t \in [0, 1]$, with $F = 4$ sub-intervals

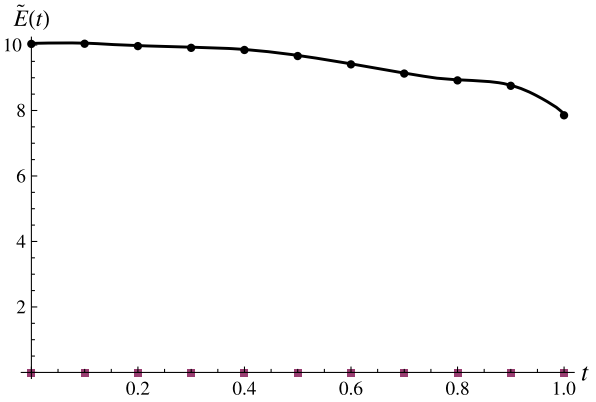

Fig. 4 Total elastic energy $\tilde{E}(t)$ plotted versus time. Squared markers on the x-axis denote the grid points $t_f \in [t_0, t_{\text{fin}}]$ where the constraint (24) is enforced

markers on the x-axis denote the grid points where the constraint (26) is enforced. In Fig. 7, the behaviors of Lk, Wr(t), and Tw(t) are shown: Lk is constant and equal to 3 as expected, and as t increases, the twist Tw(t) is converted in writhe Wr(t) according to (12). The coiling induced by filament folding is also measured by the growth in total curvature $\mathcal{K}(t)$ plotted in Fig. 8. Both $\mathcal{K}(t)$ and Wr(t) increase in time. Con-

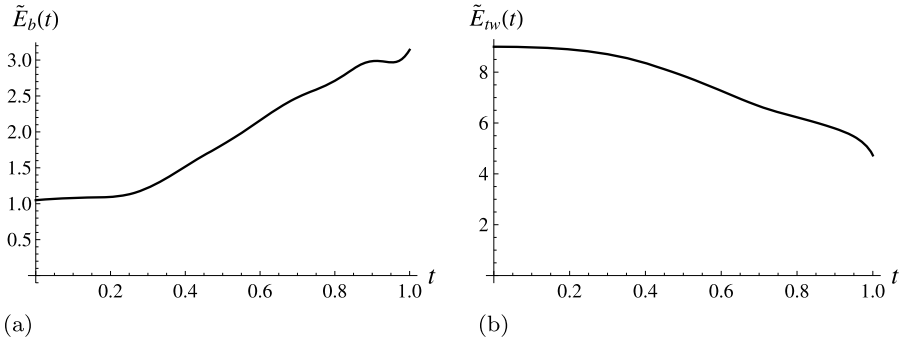

Fig. 5 (**a**) Bending energy $\tilde{E}_b(t)$ and (**b**) mean twist energy $\tilde{E}_{tw}(t)$ plotted versus time

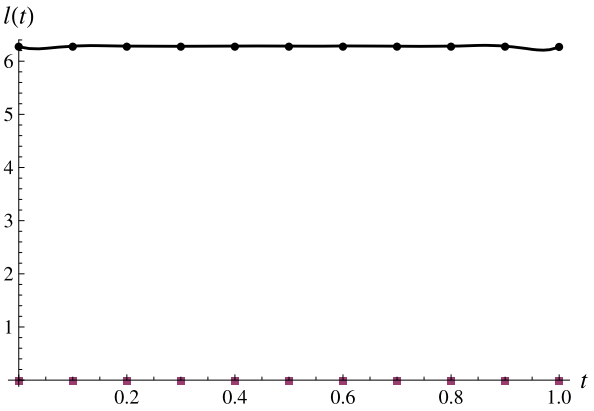

Fig. 6 Filament length function $l(t)$ versus time. Squared markers on the x-axis denote the grid points $t_f \in [t_0, t_{\text{fin}}]$ where the constraint (26) is enforced

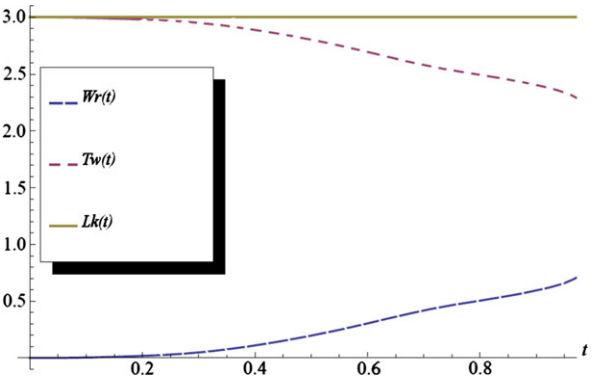

Fig. 7 Evolution of Wr(t), Tw(t), and Lk versus time

tributions to the total twist Tw(t) from normalized total torsion $\mathcal{T}$ and intrinsic twist $\mathcal{N}$ according to the decomposition (11) are plotted in Fig. 9, showing the conversion of one of the three initial units of intrinsic twist (since initial conditions are given by $\mathcal{T} = 0$ and $\mathcal{N} = 3$) to total torsion at $t = 0.3$. The conversion is associated with the passage through an inflexional configuration (see Fig. 10) characterized by the

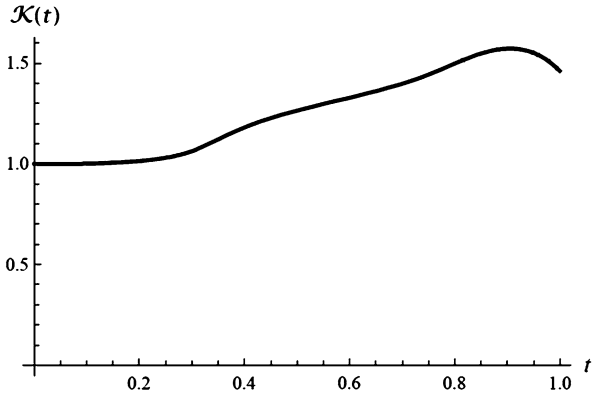

Fig. 8 Evolution of total curvature $\mathcal{K}(t)$ versus time

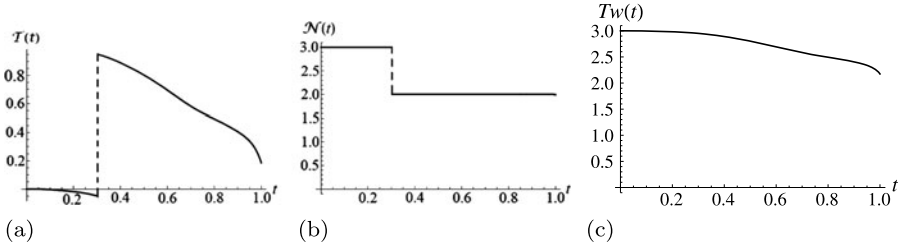

Fig. 9 (**a**) Normalized total torsion $\mathcal{T}(t)$ and (**b**) normalized intrinsic twist $\mathcal{N}(t)$ versus time. Note that at the passage through the inflexional configuration at $t = 0.3$ the discontinuities in $\mathcal{T}$ and $\mathcal{N}$ compensate, so $\mathrm{Tw}(t) = \mathcal{T}(t) + \mathcal{N}(t)$ (**c**) is still a smooth function in space and time

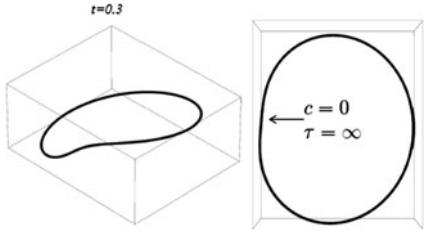

Fig. 10 Side and top view of the occurrence at $t = 0.3$ of an inflexional configuration characterized by point on the curve with zero curvature

occurrence of a point on the curve with zero curvature and local change of concavity of the curve. At the point of inflexion the torsion is singular, but the singularity is integrable and the contribution from the integral of the total torsion through the inflexional state involves a jump $[\mathcal{T}] = 1$ in total torsion that must be compensated by an equal and opposite jump in the intrinsic twist $\mathcal{N}$, so that Tw remains a smooth function in space and time [8, 36]. All the graphics described refer to the kinematics solution depicted in Fig. 11 which shows the evolution of the initial circular configuration towards an energetically preferable final state. From a topological viewpoint, the single coil formation evolutions studied in [8], whether the generatrix curve is epicycloid or a hypocycloid, and the one depicted in Fig. 11 are equivalent; there are, however, marked differences in the geometric way the coil forms. In the case of an epicycloid generatrix, the filament writhes and coils simultaneously through one

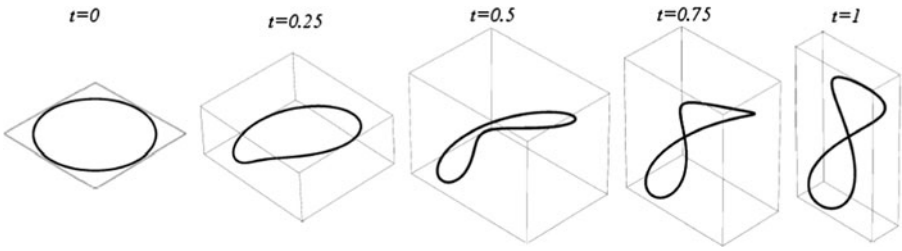

Fig. 11 Side view of one coil formation solution by means of the cubic B-spline representation method depicted in $[t_0, t_{\text{fin}}] = [0, 1]$ with time step $q = 0.25$

deformation and the coil springs from a localized loop region and grows out in the interior region; in the case of a hypocycloid generatrix, there are three distinct locations where loop deformation occurs, from each of which a single coil develops and only one survives to form the final coil, since eventually two of them coalesce in a single arc. On the other hand, the solution depicted in Fig. 11 shows a filament that writhes through one deformation region as in epicycloid generatrix but developing into the final figure-eight interwound associated with conversion of mean twist energy into bending energy.

Convergence has been tested in space and time, by modifying the number of discretization points and the size of the time step. Convergence in time has been tested by ranging the time step from 0.05 to 0.5; note that for an increasing number of discretization points (and, consequently, larger number of variables), the solvers used perform poorly and the solution variables show a random behavior. Future research will plan to develop a specific solver addressed for this problem. Convergence in space has been tested by dividing the curve from 5 to 30 segments. Convergence for different values of the smoothing parameters $\gamma \in [0, 0.1]$ and $\mu \in [0, 0.1]$ has been also tested showing a regular behavior of the solution choosing $\mu < \gamma$ with $\gamma = 0.1$.

7 Conclusions and Future Works

In this paper, kinematics of looping of a closed filament are obtained by solving the corresponding elastic energy minimization problem. The proposed model is applied to the case of single coil formation and it requires a monotonic decreasing behavior in time of the elastic energy in terms of bending and twisting contributions; it includes constraints to ensure fixed contour length of the filament and prescribed initial condition on critical twist value to generate the coiling. Time evolution functions are described by means of piecewise polynomial transformations based on cubic B-spline functions considering the corresponding de Boor control points as the unknowns in a nonlinear optimization problem. This represents the main contribution of the paper with respect to the companion articles [8] and [9], where time dependence has been prescribed to investigate geometric features associated with the coiling process.

The results show the energetic exchange between the initial circle and the final figure-eight interwound associated with conversion of mean twist energy into bending energy. Geometric characteristics of the filament evolution such as writhing number,

normalized total curvature, and twist, in terms of its contributions from normalized total torsion and intrinsic twist, have been analyzed in relation to the passage through an inflexional configuration involving a localized distortion of the filament fibers.

Note that a more general approach to find a set of possible configurations linked isotopically to the twisted ring rather than (3) should be obtained by defining the kinematics with respect to an orthonormal frame $(\hat{\mathbf{d}}_1, \hat{\mathbf{d}}_2, \hat{\mathbf{d}}_3)$ defined for the axis curve $\mathcal{C}$ in the following way:

$$\boldsymbol{\omega}(\xi, t) = u_1(\xi, t)\mathbf{d}_1(\xi, t) + u_2(\xi, t)\mathbf{d}_2(\xi, t) + u_3(\xi, t)\mathbf{d}_3(\xi, t), \tag{38}$$

$$\mathbf{d}_i'(\xi, t) = \boldsymbol{\omega}(\xi, t) \times \mathbf{d}_i(\xi, t), \quad i = 1, 2, 3. \tag{39}$$

Specification of the functions $u_i(\xi, t), i = 1, 2, 3$ and of a set of initial conditions is sufficient to specify the rod morphology. The filament geometry can be then reconstructed at all times by integrating the tangent vector:

$$\mathbf{X}(\xi, t) = \int_0^{\xi} \hat{\mathbf{d}}_3(\xi, t)\, \mathrm{d}\xi. \tag{40}$$

It would presumably be a much more difficult problem as it would be necessary to solve the linear differential equation associated with (38) to calculate the writhe. However, this approach would offer a more general set of possible configuration linked isotopically to the twisted ring.

Future research will aim to extend the investigation including both elastic potential and electrostatic forces to model the behavior of the filament in a solvent, particularly important for DNA applications. We also plan to develop a specific solver addressed for this problem able to solve a large scale optimization problem associated to multiple coils and knots formation, relevant in biological systems [37, 38].

Acknowledgements F. Maggioni would like to thank Renzo L. Ricca and David Swigon for discussions and helpful advices.

References

1. Bauer, W.R., Crick, F.H.C., White, J.H.: Supercoiled DNA. Sci. Am. **243**, 100–113 (1980)
2. Stasiak, A., Circular, D.NA.: In: Semlyen, J.A. (ed.) Large Ring Molecules, pp. 43–97. Wiley, New York (1996)
3. Cozzarelli, N.R., Wang, J.C. (eds.): DNA Topology and Its Biological Effects. Cold Spring Harbor Laboratory Press, New York (1990)
4. Demurtas, D., Amzallag, A., Rawdon, E.J., Maddocks, J.H., Dubochet, J., Stasiak, A.: Bending modes of DNA directly addressed by cryo-electron microscopy of DNA minicircles. Nucleic Acids Res. **37**(9), 2882–2893 (2009)
5. Víglasky, V., Valle, F., Adamcík, J., Joab, I., Podhradsky, D., Dietler, G.: Anthracycline-dependent heat-induced transition from positive to negative supercoiled DNA. Electrophoresis **24**(11), 1703–1711 (2003)
6. Amzallag, A., Vaillant, C., Jacob, M., Unser, M., Bednar, J., Kahn, J.D., Dubochet, J., Stasiak, A., Maddocks, J.H.: 3D reconstruction and comparison of shapes of DNA minicircles observed by cryo-electron microscopy. Nucleic Acids Res. **34**(18), e125 (2006)
7. Wiggins, P.A., van der Heijden, T., Moreno-Herrero, F., Spakowitz, A., Phillips, R., Widom, J., Dekker, C., Nelson, P.: High flexibility of DNA on short length scales probed by atomic force microscopy. Nat. Nanotechnol. **1**, 137–141 (2006)

8. Maggioni, F., Ricca, R.L.: Writhing and coiling of closed filaments. Proc. R. Soc. A **462**, 3151–3166 (2006)
9. Ricca, R.L., Maggioni, F.: Multiple folding and packing in DNA modeling. Comput. Math. Appl. **55**, 1044–1053 (2008)
10. Michell, J.H.: On the stability of a bent and twisted wire. Messenger Math. **11**, 181–184 (1989/1990)
11. Zajac, E.E.: Stability of two planar loop elasticas. J. Appl. Mech. **29**, 136–142 (1962)
12. Goriely, A.: Twisted elastic rings and the rediscoveries of Michell's instability. J. Elast. **84**, 281–299 (2006)
13. Benham, C.J.: Onset of writhing in circular elastic polymers. Phys. Rev. A **39**, 2582–2586 (1989)
14. LeBret, M.: Twist and writhing in short circular DNA according to first-order elasticity. Biopolymers **23**, 1835–1867 (1984)
15. Fuller, F.B.: The writhing number of a space curve. Proc. Natl. Acad. Sci. USA **68**, 815–819 (1971)
16. Coleman, B.D., Swigon, D.: Theory of supercoiled elastic rings with self-contact and its application to DNA plasmids. J. Elast. **60**, 171–221 (2000)
17. Coleman, B.D., Swigon, D., Tobias, I.: Elastic stability of DNA configurations. II. Supercoiled plasmids with self-contact. Phys. Rev. E **61**, 759–770 (2000)
18. Coleman, B.D., Tobias, I., Swigon, D.: Theory of influence of end conditions on self-contact in DNA loops. J. Chem. Phys. **103**, 9101–9109 (1995)
19. Schlick, T., Li, B., Olson, W.K.: The influence of salt on the structure and energetics of supercoiled DNA. Biophys. J. **67**(6), 2146–2166 (1994)
20. Timothy, P., Westcott, I.T., Olson, W.K.: Modeling self-contact forces in the elastic theory of DNA supercoiling. J. Chem. Phys. **107**, 3967 (1997)
21. Goriely, A., Tabor, M.: The nonlinear dynamics of filaments. Nonlinear Dyn. **21**, 101–133 (2000)
22. Goriely, A., Nizette, M., Tabor, M.: On the dynamics of elastic strips. J. Nonlinear Sci. **11**, 3–45 (2001)
23. Klapper, I.: Biological applications of the dynamics of twisted elastic rods. J. Comput. Phys. **125**, 325–337 (1996)
24. Schlick, T.: Modeling superhelical DNA: recent analytical and dynamical approaches. Curr. Opin. Struct. Biol. **5**, 245 (1995)
25. Schlick, T., Olson, W.K.: Supercoiled DNA energetics and dynamics by computer simulation. J. Mol. Biol. **223**, 1089–1119 (1992)
26. Arganbright, D.E.: Practical Handbook of Spreadsheet Curves and Geometric Constructions. CRC Press, Boca Raton (1993)
27. Lockwood, E.H.: A Book of Curves. Cambridge University Press, Cambridge (1961)
28. Kauffman, L.H.: Fourier Knots (1997). arXiv:q-alg/9711013v2
29. Kamien, R.D.: The geometry of soft materials: a primer. Rev. Mod. Phys. **74**, 953–971 (2002)
30. Călugăreanu, G.: Sur les classes d'isotopie des nœuds tridimensionnels et leurs invariants. Czechoslov. Math. J. **11**, 588–625 (1961)
31. White, J.H.: Self-linking and the Gauss integral in higher dimensions. Am. J. Math. **91**, 693–728 (1969)
32. Ricca, R.L.: The energy spectrum of a twisted flexible string under elastic relaxation. J. Phys. A, Math. Gen. **28**, 2335–2352 (1995)
33. Atkinson, K.E.: An Introduction to Numerical Analysis. Wiley, New York (1989)
34. de Boor, C.: A Practical Guide to Splines. Applied Mathematical Sciences, vol. 27. Springer, New York (1978)
35. Nocedal, J., Wright, S.J.: Numerical Optimization. Springer Series in Operations Research. Springer, New York (1999)
36. Moffatt, H.K., Ricca, R.L.: Helicity and the Călugăreanu invariant. Proc. R. Soc. Lond. Ser. A, Math. Phys. Sci. **439**, 411–429 (1992)
37. Sumners, D.W.: Random knotting: theorems, simulations and applications. In: Ricca, R.L. (ed.) Lectures on Topological Fluid Mechanics. Lecture Notes in Mathematics, vol. 187, pp. 201–231. Springer, Berlin (2009)
38. Arsuaga, J., Tan, R.K.Z., Vazquez, M., Sumners, D.W., Harvey, S.C.: Investigation of viral DNA packaging using molecular mechanics models. Biophys. Chem. **101**, 475–484 (2002)